

Accepted Manuscript

Indole-coumarin-thiadiazole hybrids: An appraisal of their MCF-7 cell growth inhibition, apoptotic, antimetastatic and computational Bcl-2 binding potential

Pooja R. Kamath, Dhanya Sunil, Manu M. Joseph, Abdul Ajees Abdul Salam, Sreelekha T. T



PII: S0223-5234(17)30393-8

DOI: [10.1016/j.ejmech.2017.05.032](https://doi.org/10.1016/j.ejmech.2017.05.032)

Reference: EJMECH 9462

To appear in: *European Journal of Medicinal Chemistry*

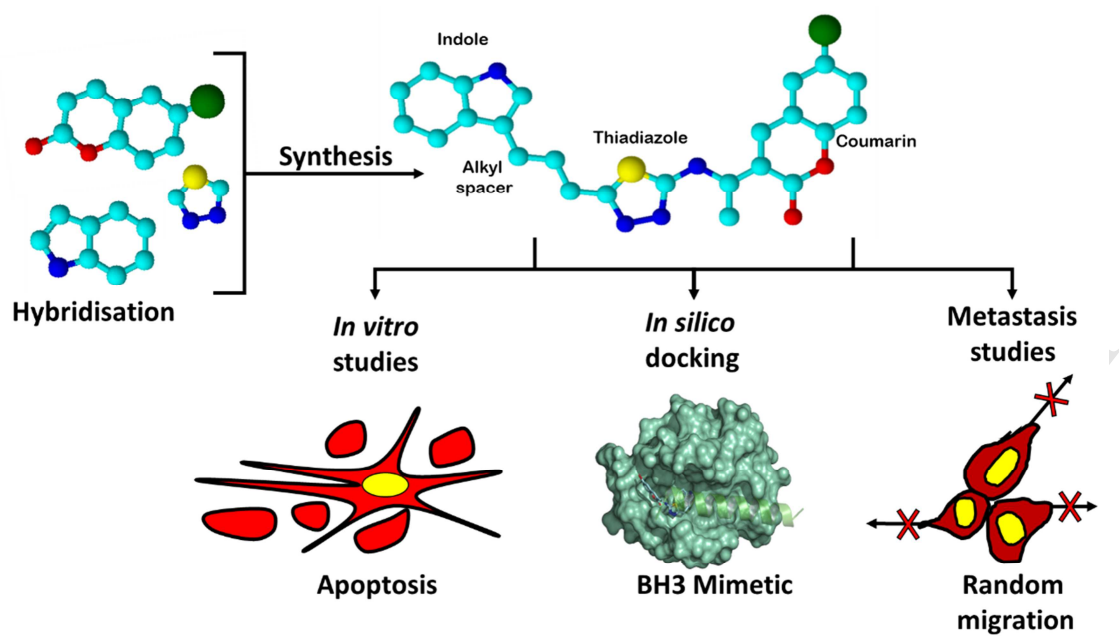
Received Date: 12 March 2017

Revised Date: 10 May 2017

Accepted Date: 11 May 2017

Please cite this article as: P.R. Kamath, D. Sunil, M.M. Joseph, A.A. Abdul Salam, S.T. T, Indole-coumarin-thiadiazole hybrids: An appraisal of their MCF-7 cell growth inhibition, apoptotic, antimetastatic and computational Bcl-2 binding potential, *European Journal of Medicinal Chemistry* (2017), doi: 10.1016/j.ejmech.2017.05.032.

This is a PDF file of an unedited manuscript that has been accepted for publication. As a service to our customers we are providing this early version of the manuscript. The manuscript will undergo copyediting, typesetting, and review of the resulting proof before it is published in its final form. Please note that during the production process errors may be discovered which could affect the content, and all legal disclaimers that apply to the journal pertain.



Indole-coumarin-thiadiazole hybrids: An appraisal of their MCF-7 cell growth inhibition, apoptotic, antimetastatic and computational Bcl-2 binding potential

Pooja R Kamath^a, Dhanya Sunil^{a*}, Manu M Joseph^b, Abdul Ajees Abdul Salam^c, Sreelekha T
T^d

^aDepartment of Chemistry, Manipal Institute of Technology, Manipal University, India.

^bChemical Sciences & Technology Division (CSTD), CSIR - National Institute for Interdisciplinary Science & Technology (NIIST), India.

^cDepartment of Atomic and Molecular Physics, Manipal University, India.

^dLaboratory of Biopharmaceuticals and Nanomedicine, Division of Cancer Research, Regional Cancer Centre, India.

* Address for correspondence

Dhanya Sunil

Department of Chemistry,

Manipal Institute of Technology,

Manipal-576104, India.

Tel. +91 820 2924412

Email: dhanyadss3@gmail.com

Indole-coumarin-thiadiazole hybrids: An appraisal of their MCF-7 cell growth inhibition, apoptotic, antimetastatic and computational Bcl-2 binding potential

Abstract:

Cancer therapeutic potential of thiadiazole hybrids incorporating pharmacologically active indole and coumarin moieties have not been explored much. In the current investigation, three new thiadiazole hybrids with spacers of varying lengths linking indole and thiadiazole units were synthesized and their structures were well-established using various spectroscopic techniques. 3-(1-(5-(3-(1*H*-indol-3-yl)propyl)-1,3,4-thiadiazol-2-ylimino)ethyl)-6-bromo-2*H*-chromen-2-one (**IPTBC**) exhibited dose-dependent cytotoxicity in breast adenocarcinoma (MCF-7) cells. The circumvention of apoptosis is a prominent hallmark of cancer and hence triggering apoptosis in specific cancer cells is one of the convenient and widely used approaches for the development of anticancer chemotherapeutics. The induction of apoptosis upon treatment with **IPTBC** was confirmed by multiple apoptosis assays like Acridine orange-ethidium bromide, Hoechst staining, TUNEL staining, and colorimetric quantification using APOPercentageTM Apoptosis assay. The apoptosis initialisation through the active involvement of caspases was confirmed by caspase profiling tests. The wound healing assay displayed an intense impairment in the motility of MCF-7 cells suggesting the anti-metastatic potential of **IPTBC**. The ability of **IPTBC** to inhibit the antiapoptotic Bcl-2 protein by acting as a small molecule BH3 mimetic was explored through docking simulation studies. Although auxiliary investigations are warranted with this promising thiadiazole hybrid **IPTBC**, the perspective anticancer potential through programmed cell death, anti-metastatic and probable Bcl-2 inhibitory action will enable its further exploration in oncology.

Keywords: Apoptosis; Bcl-2; Cell cycle; Cytotoxicity; IPTBC; Metastasis.

1. Introduction

Cancer, characterized by a lack of cell death and increased cell proliferation rate results from a series of genetic mutations. The well-orchestrated apoptosis process where cells are programmed to die in response to specific stimuli is crucial for sustaining the physiologic balance between cell growth and cell death [1]. This complex process of apoptosis is generally achieved by two key pathways: extrinsic pathway that involves the binding of death ligands to death receptors or intrinsic pathway modulated through mitochondrial contribution [2]. Apoptosis is characterized by distinctive morphological alterations, like chromatin condensation, nuclear fragmentation, membrane blebbing [3], and various biochemical modifications that include caspase activation and membrane surface variations that permit the apoptotic bodies to be recognized and engulfed by phagocytes [4]. Disruption of these apoptotic mechanisms often leads to cancer development and resistance to cancer chemotherapy. The increasing knowledge on these apoptotic pathways and the development of few molecules that trigger apoptosis in malignant cells advocates that cell death can be targeted therapeutically. However, the major problem that limits effective cancer treatment may be a lack of tumor specificity of drugs, development of drug resistance and activation of proliferation pathways or resistance of cancer cells to death stimuli. Various approaches to circumvent tumor resistance include activation of death receptor-mediated extrinsic pathway through proapoptotic receptors, restoration of p53 activity, inhibition of Bcl-2 family antiapoptotic proteins, caspase modulation by targeting intracellular caspase inhibitors etc [5].

Medicinal chemistry faces a major challenge in designing new synthetic compounds with appropriate therapeutic importance. Molecular designing by incorporation of various biologically active heterocyclic pharmacores into one single molecule could be a source of benefit for emerging hybrid molecules with interesting and versatile biological potential [6]. Hence a hybrid multifunctional molecule carrying more than one pharmacophoric entity, wherein each individual active unit exerts diverse modes of action could be more beneficial in cancer treatment. 1,3,4-Thiadiazole moiety has many desirable features which permit it to occupy a major position among the most common FDA-approved marketed drugs [7]. Its vast array of pharmaceutically suitable biological activities is attributed to the presence of the =N-C-S group, a hydrogen binding domain with two electron donor system together with an additional involvement of the sulphur atom that improves the lipo-solubility of the molecule [7-9]. As oxygen and nitrogen based heterocyclic scaffolds: coumarin and indole, exhibits approving responses as anticancer agents, [10-13] these pharmacophores were structurally

modified to unite with the 1,3,4-thiadiazole moiety to design new polycyclic scaffolds. In the present study, three new hybrid derivatives with bioactive indole, coumarin and 1,3,4-thiadiazole units were synthesized and examined for their impact on selective cytotoxicity in breast adenocarcinoma cells and their efficacy in triggering apoptosis and restricting cancer cell migration. The probable mechanistic pathway of cell death was also probed using caspase expression studies and computational docking studies with anti-apoptotic protein Bcl-2 as target receptor.

2. Materials and methods

All chemicals procured from Sigma Aldrich, Merck India and Himedia, were of reagent grade and used without further purification. The progress of the synthetic reactions was monitored by thin layer chromatography using pre coated aluminium sheets with Aluchrosep silica Gel 60/ UV₂₅₄ and spot visualization was done in a UV chamber. IR spectra were recorded on a Shimadzu 8400S FTIR spectrometer. ¹H and ¹³C NMR were recorded in Bruker 400 MHz spectrometer and mass spectra in a Shimadzu GCMS-QP5050 spectrometer. Melting points were determined by the open capillary method and are uncorrected. Elemental analysis was carried out using a Flash thermo 1112 series CHN analyser.

2.1. Chemistry

Indole 3-carboxylic acids with various alkyl spacers (n = 1 to 3) were chosen as the starting compounds and were condensed with thiosemicarbazide using POCl₃ as cyclizing agent [14] to obtain three 5-(1*H*-indol-3-ylalkyl)-1,3,4-thiadiazol-2-amines. 3-Acetyl-6-bromo coumarin-2-one was prepared by the cyclization reaction of substituted 5-bromo-2-hydroxybenzaldehyde and ethyl-acetoacetate using the/a catalytic amount of piperidine via sonication for about 30 min at 60°C [15]. The final three hybrid molecules were synthesized by the condensation reaction between 5-(1*H*-indol-3-ylalkyl)-1,3,4-thiadiazol-2-amines and 3-acetyl-6-bromo coumarin-2-one. The synthetic pathway is depicted in scheme 1.

Scheme-1

2.2. *In-vitro* anticancer studies

2.2.1. Cell lines and cell culture

Human breast adenocarcinoma (MCF-7) and normal kidney epithelial (Vero) cell lines of *Cercopithecus aethiops* were obtained from National Centre for Cancer Sciences, Pune, India. Both the cell lines were well-maintained in T-75 cm² flasks (Falcon, Becton Dickinson, USA) in Dulbecco's modified Eagles medium (DMEM - catalogue # AT-151, HiMedia, Mumbai, India) supplemented with 10% Fetal bovine serum (FBS - catalogue # RM 9955, HiMedia, Mumbai, India) along with a mixture of antibiotics (1 µg/L of streptomycin, 0.25µg amphotericin B and 1 U/mL of penicillin). Cells were maintained in 5 % CO₂ incubator at 37°C to attain 70-80% cell confluence.

2.2.2. MTT assay

The growth inhibition effects of the three newly synthesized molecules were assessed using MTT assay based on the reduction of MTT dye by live MCF-7 and Vero cell lines. The working solutions of varying concentrations were prepared by dilution of stock solutions (25 mM DMSO solution) of test hybrids using DMEM. Commercially available vincristine solution (1 mM, Cipla, India) diluted in DMEM directly was used as positive control in all the experiments.

Briefly, about 5×10^3 cells were seeded in 96-well plate and cultured overnight by incubating at 37 °C in a 5% CO₂ atmosphere. After 24 h, cells were exposed to different concentrations of hybrid compounds or positive control vincristine and were incubated further for 48 h. The media containing test compounds was discarded, MTT reagent (1 mg/mL) was added to the cells and incubated for another 4 h at 37°C. The formazan crystals developed was dissolved in DMSO and the absorbance was recorded using a multiplate (Tecan M200, Austria) reader at 570 nm [16]. As the stock solutions of the compounds were initially prepared in DMSO, suitable DMSO vehicle controls were included. The percentage of viable cells were calculated using the formula:

$$\% \text{ Cell viability} = \frac{\text{Test absorbance} - \text{Blank absorbance}}{\text{Vehicle control absorbance} - \text{Blank absorbance}} \times 100$$

2.2.3. Acridine orange-ethidium bromide (AO/EtBr) dual staining

Morphological evaluation of apoptosis based on the differential uptake of AO and EtBr by viable and nonviable cells was performed in MCF-7 cells treated with test compound for 24 h. Initially, cells were viewed under phase contrast objective of an inverted fluorescent microscope (Olympus 1X51, Singapore) and observed for any visible gross apoptotic

morphological changes on treatment with the test molecule for 24 h [17]. Later, cells were treated with test compound in a 96-well plate and incubated for 24 h at 37°C in 5% CO₂ atmosphere [18, 19]. After incubation, media was removed and 25 µL of DNA binding fluorescent AO (7.5µg) / EtBr (25 µg) stain was added, mixed well and examined under fluorescent microscope, using an FITC filter (Olympus 1X51, Singapore).

2.2.4. Hoechst staining

Hoechst 33342 cell-permeate nuclear counterstaining was used to observe the nuclei for any apoptosis related changes like nuclear condensation and DNA fragmentation. The cells were examined under an inverted fluorescence microscope using a DAI filter (Olympus1X51, Singapore) [20]. The cells treated with test compound were incubated with Hoechst stock solution (1:2,000) in phosphate buffer saline (PBS) for 10 min and observed for morphological changes in the nuclear DNA upon comparison with the vehicle control cells.

2.2.5. TUNEL staining

TUNEL assay (DeadEnd™ fluorometric TUNEL system – G3250, Promega, Madison, WI, USA) was employed to identify the incorporation of the fluorescein-12-dUTP at 3'-OH DNA ends in the fragmented DNA of apoptotic cells, using the terminal deoxynucleotidyl transferase recombinant (rTdT) enzyme as per the manufacturer's instructions with propidium iodide (PI) as counter-stain. [3]. In brief, around 1×10^5 MCF-7 cells per well taken in 24-well flat-bottom wells was treated with the test compound for 24 h. The plates were further washed with PBS, fixed with 4% paraformaldehyde, and permeabilized with 0.2% Triton X-100. Further, the cells were exposed to 50 µM fluorescein-12-dUTP, equilibration buffer, and terminal deoxynucleotidyl transferase (TdT) for about 1 h at 37°C. The reaction was ceased by washing the cells in 2×SSC (Saline-sodium citrate buffer) followed by washing twice in PBS. The cells were then counterstained with 1 mg/mL PI (Propidium Iodide), washed using dH₂O and analysed using a fluorescence microscope.

2.2.6. APOPercentage™ Apoptosis assay

Early onset of apoptosis was further monitored and colorimetrically estimated using APOPercentage™ dye (Biocolor, Belfast, Northern Ireland). Briefly, 1×10^4 MCF-7 cells were cultured in 96-well tissue culture plates and grown to sub-confluent monolayers for 48 h. The cells were incubated with test compound for 24 h, the medium was removed, and

examined after 1h incubation with a fresh culture medium comprising APOPercentage dye. The photo images of APOPercentage dye-labelled cells, which stained purple-red under a light microscope, were used to quantify the extent of apoptosis. The cells were lysed and the dye uptake was quantified by colorimetric method according to the manufacturer's instruction [4]. The absorbance was measured at 550 nm using a microplate reader (Biotek, USA).

2.2.7. Caspase profiling

The impact of the test compound on the expression of initiator caspases (caspases 2, 8 and 9) was studied by using Apo Alert™ Caspase Profiling kit (Clontech, CA, USA) as per the manufacturer's protocol [20]. Cells were exposed to the test molecule for 24 h, and samples were transferred to 96-well plates for fluorimetric reading (λ_{ex} 380 nm, λ_{em} 460 nm). The signals were recorded by spectrofluorimetry (FLx800, BioTek).

2.2.8. Monolayer wound healing migration assay

The migration of MCF-7 cells which is vital to cancer invasion and later metastasis was monitored using wound healing assay [21]. A scratch was created in a cell monolayer and the cell motility towards the centre of the wound gap was examined. About 1×10^5 cells/well containing DMEM was seeded to 80% confluence, media was aspirated and a single scratch was created. The cellular debris was washed with PBS and the cells were treated with positive control vincristine/test molecule. The experiment was performed in triplicates. The extent of wound closure was visualized using microscope stage micrometer and an eye piece micrometer at 45X objective. The digital images were taken with a CCD camera attached to inverted microscope (Nikon Eclipse TS100).

2.2.9. Statistical Analysis

The results of the study performed are expressed as the Mean \pm Standard Deviation. All the analyses were carried out with GraphPad Prism (CA, USA). The statistical significance was considered at $p < 0.05$.

2.3. *In silico* docking studies

In silico computational docking studies were executed using AutoDock Vina [22] and the input files needed for docking studies were arranged using AutoDock Tools [23]. The X-ray

crystallographic structures of Bcl-2 from Protein Data Bank (PDB) ID: 2XA0 was selected as a receptor for generating docking simulations. Water and ligand molecules bound with the proteins were removed and the monomer model was selected for molecular docking studies with the active hybrid molecule. The receptor was kept rigid, while torsional bonds of the hybrid ligand were set flexible to rotate to explore the most plausible binding positions. The grid covering all the amino acids present inside the binding pocket was built at the centre of the active pocket for Bcl-2 (24 x 22 x 20 points in x,y,z direction and 37, -20 and -16 as grid centre). Protein-ligand complex was predicted using Autodock Vina with the pdbqt format files for both protein and ligand. Each docking calculation was repeated thrice using three different seeds, and the remaining values retained as default. Final models were chosen based on the affinity as well as the molecular contacts. The hydrophobic contacts, hydrogen bonds and other molecular interactions were calculated using Protein-Ligand Interaction Profiler (<https://projects.biotech.tu-dresden.de/plip-web/plip/index>) and PoseView online software (<http://poseview.zbh.uni-hamburg.de/>). The figures were generated using Pymol (<http://www.pymol.org>) and PoseView.

3. Results and discussion

3.1. Chemistry

The structures of the synthesized compounds were established by IR, NMR and mass spectra and CHN data. All synthesized compounds presented IR absorption bands spanning from 3200 to 3400 cm^{-1} for N-H stretching, 3040 to 3050 cm^{-1} for C-H aromatic stretching, two symmetric and asymmetric stretching absorption bands each around 2950 and 2850 cm^{-1} , carbonyl stretching of lactone at 1730 cm^{-1} , C=N stretching around 1670 cm^{-1} and C-Br stretching band at 560 cm^{-1} . The ^1H NMR spectra of, all the three hybrids displayed prominent singlets due to CH_3 protons at around 2.5 ppm. The aromatic protons were observed resonating around 6.9-8.7 ppm. The alkyl protons that links indole and thiaziazole rings appeared as a singlet at δ 4.23 (n=1), two triplets around 3.2 to 3.4 (n=2) and two triplets and one multiplet from 2.1 to 3 ppm (n=3). The indole NH resonated as a broad singlet at δ 11. The ^{13}C NMR spectra showed two peaks around 195 and 166 ppm for the highly deshielded carbon atoms present in the thiaziazole ring. The aromatic carbons were observed in the range 111 to 158 ppm while the aliphatic carbons between 21 to 39 ppm. The mass spectra of all the synthesized hybrids were in agreement with their respective molecular

formulae. The percentages of elements in CHN analysis were well within the permissible limits.

Experimental

3-(1-(5-((1*H*-indol-3-yl)methyl)-1,3,4-thiadiazol-2-ylimino)ethyl)-6-bromo-2*H*-chromen-2-one (IMTBC)

Brown solid (85 %); m.p. 182-184 °C; IR (KBr) [cm⁻¹]: 3390 (N-H *str.*), 3051 (Ar. C-H *str.*), 2983 (methyl C-H *asym. str.*), 2827 (methyl C-H *sym. str.*), 1735 (lactone C=O *str.*), 1676 (C=N *str.*), 1602, 1550 (Ar. C=C *str.*), 1355 (Ar. C-O-C *str.*), 559 (C-Br *str.*); ¹H NMR (400 MHz, DMSO-d₆) [ppm]: δ 2.58 (s, 3H, CH₃), δ 4.23 (s, 2H, CH₂), δ 6.92-6.96 (t, 2H, indole 5-H & 6-H), δ 7.28 (s, 1H, indole 2-H), δ 7.35-7.36 (d, 1H, coumarin 8-H), δ 7.44-7.46 (d, 2H, indole 4-H & 7-H), δ 7.88-7.90 (d, 1H, coumarin 7-H), δ 8.22 (s, 1H, coumarin 4-H), δ 8.61 (s, 1H, coumarin 5-H), δ 10.98 (s, 1H, indole N-H); ¹³C NMR (100 MHz, DMSO-d₆) δ = 26.55, 30.48, 111.28, 112.01, 116.83, 118.81, 118.88, 119.07, 120.53, 121.71, 124.09, 125.89, 127.05, 133.00, 136.77, 137.06, 146.10, 150.01, 154.09, 158.47, 167.17, 195.47; MS (m/z): 480 (M+1), 482 (M+3); Anal. Calcd. for C₂₂H₁₅N₄BrO₂S: C, 55.12; H, 3.15; N, 11.69; found: C, 55.34; H, 3.17; N, 11.71.

3-(1-(5-(2-(1*H*-indol-3-yl)ethyl)-1,3,4-thiadiazol-2-ylimino)ethyl)-6-bromo-2*H*-chromen-2-one (IETBC)

Brown solid (74%); m.p. 210-212 °C; IR (KBr) [cm⁻¹]: 3338 (N-H *str.*), 3043 (Ar. C-H *str.*), 2923 (methyl C-H *asym. str.*), 2852 (methyl C-H *sym. str.*), 1735 (lactone C=O *str.*), 1676 (C=N *str.*), 1608, 1550 (Ar. C=C *str.*), 1357 (Ar. C-O-C *str.*), 559 (C-Br *str.*); ¹H NMR (400 MHz, DMSO-d₆) [ppm]: δ 2.57 (s, 3H, CH₃), δ 3.28-3.30 (t, 2H, CH₂), δ 3.36-3.38 (t, 2H, CH₂), δ 6.91-6.95 (t, 2H, indole 5-H & 6-H), δ 7.26 (s, 1H, indole 2-H), δ 7.34-7.35 (d, 1H, coumarin 8-H), δ 7.43-7.45 (d, 2H, indole 4-H & 7-H), δ 7.87-7.89 (d, 1H, coumarin 7-H), δ 8.21 (s, 1H, coumarin 4-H), δ 8.60 (s, 1H, coumarin 5-H), δ 10.96 (s, 1H, indole N-H); ¹³C NMR (100 MHz, DMSO-d₆) δ = 26.54, 30.43, 32.89, 111.28, 112.00, 116.81, 118.83, 118.87, 119.07, 120.52, 121.70, 124.08, 125.87, 127.03, 133.01, 136.77, 137.05, 146.09, 149.00, 154.08, 158.47, 166.17, 195.32; MS (m/z): 493 (M+1), 495 (M+3); Anal. Calcd. for C₂₃H₁₇N₄BrO₂S: C, 55.99; H, 3.47; N, 11.36; found: C, 56.08; H, 3.48; N, 11.38.

3-(1-(5-(3-(1H-indol-3-yl)propyl)-1,3,4-thiadiazol-2-ylimino)ethyl)-6-bromo-2H-chromen-2-one (IPTBC)

Brown solid (89 %); m.p. 142-144 °C; IR (KBr) [cm⁻¹]: 3263 (N-H *str.*), 3041 (Ar. C-H *str.*), 2923 (methyl C-H *asym. str.*), 2854 (methyl C-H *sym. str.*), 1735 (lactone C=O *str.*), 1674 (C=N *str.*), 1606, 1548 (Ar. C=C *str.*), 1355 (Ar. C-O-C *str.*), 557 (C-Br *str.*); ¹H NMR (400 MHz, DMSO-d₆) [ppm]: δ 2.16 -2.18 (m, 2H, CH₂), δ 2.59 (s, 3H, CH₃), δ 2.71-2.74 (t, 2H, CH₂), δ 2.94-2.96 (t, 2H, CH₂), δ 6.99-7.03 (t, 1H, indole 5-H), δ 7.06-7.10 (t, 1H, indole 6-H), 7.31 (s, 1H, indole 2-H), δ 7.35-7.37 (d, 1H, coumarin 8-H), δ 7.44-7.47 (d, 2H, indole 4-H & 7-H), δ 7.89-7.91 (d, 1H, coumarin 7-H), δ 8.23 (s, 1H, coumarin 4-H), δ 8.61 (s, 1H, coumarin 5-H), δ 11.00 (s, 1H, indole N-H); ¹³C NMR (100 MHz, DMSO-d₆) δ = 21.32, 25.17, 30.49, 38.59, 113.23, 116.82, 118.88, 120.11, 120.54, 121.65, 125.89, 126.65, 128.44, 129.74, 131.64, 133.01, 137.06, 138.39, 146.11, 148.17, 154.09, 158.47, 164.53, 195.45; MS (m/z): 507 (M+1), 509 (M+3); Anal. Calcd. for C₂₄H₁₉N₄BrO₂S: C, 56.81; H, 3.77; N, 11.04; found: C, 56.99; H, 3.78; N, 11.06.

3.2. *In vitro* anticancer studies

3.2.1. *IPTBC* exhibits differential cytotoxicity

To investigate the potential growth inhibition and cell line specificity of the three hybrid molecules, MTT assay was performed on MCF-7 and Vero cells. The hybrid **IPTBC** linking the indole and thiadiazole pharmacores via a three methylene spacer (n=3) displayed differential cytotoxicity in MCF-7 cells compared to Vero-cells with IC₅₀ values of 8.01 μM in MCF-7 and 116.02 μM in Vero cells respectively. **IMTBC** and **IETBC** did not exhibit any marked differential cytotoxicity as evident from their IC₅₀ values of 82.1 and 36.07 μM in MCF-7 and 113.4 and 43.1 μM in Vero cells correspondingly. The results revealed the impact of one, two and three methylene spacers positioned between the indole and thiadiazole ring on the cytotoxic efficacy of hybrid molecules. The presence of three methylene linker was found to exert maximum cytotoxicity in the MCF-7 cells as reflected by the IC₅₀ values. Hence **IPTBC** was taken up for various apoptotic screening studies. Commercially available vincristine solution (1 mM, Cipla, India) was used as positive control.

3.2.2. *IPTBC* induces apoptosis in MCF-7 cells

The significantly low IC₅₀ value and differential cytotoxic behaviour make **IPTBC** an attractive candidate for exploring the mechanism of cell death pattern. Even though every

type of targeted cytotoxicity are acceptable, a programmed cell death pathway through the effective mediation of caspases is more admirable for any cytotoxic agent. In order to analyse the mechanism of cell death due to the impact of **IPTBC**, various apoptosis assays were performed after exposing MCF-7 cells to 10 μ M of **IPTBC** for 24 h.

Apoptosis is well-characterized by various morphological alterations such as chromatin condensation, DNA degradation, membrane blebbing, cell shrinkage and finally rapid phagocytosis of apoptotic debris by adjacent normal cells or macrophages [24]. Apoptosis induction by **IPTBC** in MCF-7 cells was evident from the deviations in cell morphology, loss of cell membrane integrity, shrinkage of cells and formation of apoptotic body detected during light microscopic evaluation.

AO/EtBr dual staining enabled to detect **IPTBC** induced apoptotic morphological alterations in MCF-7 cells. The nuclear morphology of the MCF-7 cells stained with fluorescent AO/EtBr for 24 h was examined under a fluorescent microscope and the representative images are depicted in Fig.1. The viable cells appeared green in colour with intact nuclei without any signs of apoptosis in the vehicle control group (Fig.1A). Whereas, the cells treated with **IPTBC** revealed a change in colour (Fig.1B) in comparison with the vehicle control and were characterized as early apoptotic (greenish yellow fluorescence and condensed chromatin), late apoptotic with condensed and fragmented nuclei (orange fluorescence), and nonviable cells (red coloured fluorescence).

Hoechst 33342 is a cell-permeable DNA stain that preferentially binds to adenine-thymine (A-T) regions of DNA and exhibits distinct fluorescence indicating the altered cellular morphology like DNA fragmentation or chromatin condensation induced by apoptotic agents. Vehicle control cells were observed uniformly light blue with round and intact nuclei (Fig.1C) under fluorescence microscope. As illustrated in Fig.1D, MCF-7 cells undergoing apoptosis due to **IPTBC** exposure for 24 h exhibited bright blue colour because of salient apoptotic changes like nuclear chromatin condensation and fragmented DNA.

Fig. 1

DNA fragmentation that leads to the formation of numerous DNA double-strand breaks with accessible 3'-hydroxyl groups is a hallmark of late event of apoptosis. Terminal deoxynucleotidyl transferase dUTP nick end labelling (TUNEL) assay was employed to detect extensive DNA degradation by labelling blunt ends of double-stranded DNA breaks.

Labelling of DNA nicks with fluorescein-12-dUTP and chromatin counterstaining with PI was done to identify the entire cell population. The nuclei of cells undergoing DNA fragmentation through apoptosis are fluorescently labelled in TUNEL assay, whereas those undergoing death as a consequence of necrosis are not. The representative photomicrographs depicting the results of TUNEL assay are presented in Fig.2A. Higher amount of TUNEL-positive (green colour) cells which are in the late apoptotic phase was detected in MCF-7 cells treated with **IPB** compared to the TUNEL- negative vehicle control.

Fig. 2

To further validate the apoptotic method of cell death prompted by **IPB** on MCF-7 cells in a non-fluorescent platform, APOPercentage™ Apoptotic assay was employed. The execution phase of apoptosis commences with the translocation of phosphatidylserine (PS) from the inner to the external surface of the cell membrane. This PS transmembrane crusade results in the uptake of the APOPercentage dye by the cells undergoing apoptosis, which lasts until the befall of blebbing, the typical characteristic of apoptosis. The representative images that depicts the results of the assay detected under a conventional microscope are shown in Fig. 3. The **IPB** treated cells that undergo apoptosis selectively incorporate the dye and are stained intensely purple-red as observed in Fig.3B. The vehicle control cells remained unstained as seen in Fig.3A. MCF-7 cells exposed to **IPB** for 24 h exhibited distinct morphological changes indicative of apoptosis like reduced cell volume, and chromatin condensation after 1 h of *in situ* staining with the dye. Besides, the concentration of the accumulated dye within the labelled cells released into solution was measured calorimetrically and the absorbance measured is quantitatively represented in Fig. 3C.

Fig. 3

Analysis of our data from multiple assays including AO/EtBr dual staining, Hoechst staining, TUNEL assay and the APOPercentage™ apoptosis assay provides the first evidence that the cell growth inhibition caused by **IPB** *in vitro*, is primarily due to apoptosis, than to necrosis. Concisely, our all experiments taken together support the inspected hypothesis that **IPB** can prompt apoptosis in *in vitro* in human breast adenocarcinoma cells.

3.2.3. **IPB** induces apoptosis via caspase cascade in MCF-7 cells

Cysteine-aspartic proteases or caspases are proteolytic enzymes which are demonstrated to perform a major role in controlling inflammation and cell death. Several anticancer drugs have been established to accomplish apoptosis via a caspase-dependent pathway. As a final approach to assess the mode of cell death, experiments were performed to determine whether the caspase proteolysis cascade is stimulated in **IPBIC** treated cells. Caspases being effective mediators of apoptosis, the expression of caspases 2, 8 and 9 was investigated by fluorimetry to validate the cell death mechanism triggered by **IPBIC**. The graph depicting the variation of the caspase levels in comparison with the vehicle control (**IPBIC** value was normalized with control and fold changes were calculated by considering control value as 1) is presented in Fig.4. Although caspase 2 was not involved in the execution of programmed cell death with **IPBIC**, the other two caspases studied are significantly altered ($p < 0.001$) in comparison with the control cells. The caspase-8 and 9 expressions in **IPBIC** treated breast cancer cells was considerably greater than that in the untreated MCF-7 cells after 24 h time point.

Fig. 4

3.3. *In silico* docking studies of ligand **IPBIC** with Bcl-2

Bcl-2 is the first apoptosis-related gene acknowledged to play a significant role in tumorigenesis and is overexpressed in a range of cancers [25]. Treatment of tumors with Bcl-2 antisense oligonucleotides and RNAi have exhibited promising potential in downregulating the protein expression and reduce tumor growth. Selective interactions of BH-3 only proteins with antiapoptotic proteins are well established [26]. Several small molecule antagonists like ABT-737 [27], ABT-263 [28], ABT-199 [29], AT-101 [30] that bind to Bcl-2 or Bcl-xL by mimicking the BH3 domain, capable of inducing apoptosis have been developed. The ability of **IPBIC** to bind into the BH3 domain of Bcl-2 was examined through computational docking simulation studies.

Bcl-2 is an anti-apoptotic member of Bcl-2 family proteins with the molecular weight of around 26 kDa (239 amino acids, UniprotKB-P10415). The binding affinities of **IPBIC** for Bcl-2 (-8.2) was measured, and the molecular interactions of the final model was compared with crystal structures of BH3 mimetic like ABT-263, ABT-199, and BAX. Docking results of ligand **IPBIC** with Bcl-2 is summarized in Table 1. In Bcl-2, **IPBIC** is bound deep inside the binding pocket (P1 hydrophobic site) in between 3_{10} and $\alpha 4$ helices

and the thiadiazole moiety engages in two hydrogen bonds with Try108 and Gln118 of Bcl-2 amino acids and seven hydrophobic interactions (Table- 1 and Fig. 5). Both the nitrogen atoms of thiadiazole moiety are involved in N-H...N (Gln118;-3.51Å) and O-H...N (Try108;-2.76 Å) hydrogen bonding with Bcl-2. The methylene spacers play a significant role in the ligand folding process. **IPBTC** has six rotatable bonds, of which the propyl unit has four, and connects both the indole and thiadiazole units. The presence of four rotatable bonds in case of propyl spacer when compared to methyl or ethyl bridge easily allows the appropriate folding of **IPBTC** that aids in favourable interactions with the target protein as revealed by the docking studies. Indole and thiadiazole units of **IPBTC** rotate by 95° with the distance of around 5Å, which facilitate Phe104 and Phe112 of Bcl-2 to make a π -stacking. Thiadiazole scaffold of **IPBTC** plays a central role in all the three kinds of interactions by making in two hydrogen bonds, hydrophobic contacts, and π -stacking. Indole moiety primarily contributes to the hydrophobic contacts and π -stacking, whereas the 6-bromo-chromen-2-one unit majorly adds to hydrophobic contacts with Ala129, Val133, and Phe153 of Bcl-2. Totally, seven amino acids of Bcl-2 (Table-1) make interactions with **IPBTC**. Moreover, the interactions of **IPBTC** bear a resemblance with ABT-263 (PDB Id: 4LVT), ABT-199 (PDB Id: 4MAN) and BAX (PDB Id: 2XA0) co-crystallized with Bcl-2. Out of the seven residues except for Arg129, all other amino acids of Bcl-2 (Tyr108, Phe104, Phe112, Gln118, Val133, Phe153) share common interactions with **IPBTC**, ABT-263, ABT-199, and BAX molecules. **IPBTC** gets itself oriented in the BH3 binding domain of Bcl-2, thereby preventing the close binding of BH-3 protein to Bcl-2 as depicted in Fig. 6. Thus **IPBTC** may act as a probable potent Bcl-2 inhibitor that can also elicit apoptosis.

Table 1: Docking interactions of **IPBTC** with Bcl-2 amino acids within 4.0Å in the binding site.

Bcl-2 Amino Acids	Ligand Moiety	Type	Distance (Å)	Angle (°)
Hydrogen Bonding				
Try108	Thiadiazole	O-H...N	2.76	133.56
Gln118	Thiadiazole	N-H...N	3.51	136.58
Hydrophobic Contacts				
Phe104	Indole		3.98	
Phe112	Thiadiazole		3.36	
Arg129	Bromo-Chromenone		3.48	

Val133	Indole		3.83	
Val133	Bromo-Chromenone		3.91	
Val133	Bromo-Chromenone		3.71	
Phe153	Bromo-Chromenone		3.68	
π-stacking				
Phe104	Indole	T	5.29	84.02
Phe112	Thiadiazole	T	5.05	89.48

Fig. 5

Fig. 6

3.4. Plausible mechanism of apoptosis induction by IPTBC

In tumorigenesis, generally apoptotic pathways are disturbed. Three major apoptosis-associated caspase activation pathways have been recognized in mammals: i) the death receptor or extrinsic pathway that operates via cell surface death receptors, ii) the mitochondria mediated intrinsic or apoptosome pathway and iii) rarely the cytotoxic lymphocyte-initiated granzyme B pathway. These apoptosis-induction pathways offer several prospective to develop potent cancer therapeutics, predominantly against multidrug resistant tumors. Both extrinsic and intrinsic pathways activate the proteolytic caspase enzyme cascade, that eventually effects in apoptosis initiation [31]. The binding of apoptosis inducing ligands with their cognate death receptors result in the formation of the death-inducing signalling complex (DISC) and trigger the extrinsic apoptotic pathway [32]. Subsequently, procaspase-8 is activated to caspase-8 through a series of events, which is further released from the DISC to activate the effector caspase-3/7 [33]. The activation of inactive procaspase-8 notably occurs through the death receptor, whereas the inhibition of Bcl-2 and activation of caspase-9 is related to mitochondrial pathway that terminates in cellular apoptosis.

Mechanistically, all our experimental data supports the induction of apoptosis by **IPTBC** probably through the activation of mitochondrial intrinsic pathway as well as death receptor/extrinsic as represented in Fig.7. However, a considerably higher level of caspase-9 expression compared to caspase-8 proposes that **IPTBC**-induced apoptosis in MCF-7 cells is

mainly through intrinsic pathway. Briefly, exposure of MCF-7 cells to **IPTBC** might induce DNA damage causing downregulated expression of anti-apoptotic protein Bcl-2. Besides, as the docking studies point towards the probable Bcl-2 inhibitory potential of **IPTBC**, it could also possibly inhibit the binding of pro-apoptotic BH-3 proteins with anti-apoptotic Bcl-2. The downregulation or inhibition of Bcl-2 could induce the activation of initiator caspase-9, most possibly through the mitochondrial release of cytochrome-c. This could trigger the caspase cascade, wherein the activated caspase -3/7 would propagate further caspase processing events, causing nuclear DNA degradation and finally apoptosis through intrinsic pathway. The literature studies demonstrate the deficiency of caspas-3 in MCF-7 cells [34]. Thus the activated caspase-7 alone, in the absence of caspase-3 might trigger the caspase flow in MCF-7 cells. Moreover, the elevated levels of caspase-8 could also recruit the mitochondrial apoptotic pathway by cleaving the BH3-only protein, BID. Cleaved BID could support BAX/BAK-dependent cytochrome c release from the mitochondria and form the apoptosome, causing caspase-9 activation and might lead to the activation of caspase-7 and thereby apoptosis via mitochondrial pathway [35, 36]. **IPTBC** may also stimulate apoptosis through interaction with putative “death receptors” in the MCF-7 plasma membrane that could promote the initial cleavage of procaspase-8, release of caspase-8 and activation of successive downstream events, that results in apoptosis probably by activating caspase-7 [32, 34].

Fig.7

In conclusion, the mitochondria dependent apoptosis triggered by **IPTBC** is thus probably initiated by caspase-8, accompanied by depolarization of the mitochondrial membrane, down-regulation of antiapoptotic Bcl-2 proteins, Bid processing, followed by release of cytochrome from the mitochondria to the cytosol and later sequential caspase cascade through effector caspase - 9, which in turn stimulates the effector caspase-7 that further leads to cell death. The death-receptor apoptosis pathway operated via caspase-8 activation could consequently activate caspase-7 but not caspase-3. However, more biochemical evidences are needed to be performed to completely substantiate the mechanism of apoptosis induced by **IPTBC**.

3.5. *IPTBC restricts migration of MCF-7 cells in vitro*

Cancer cell migration and invasion is the main feature responsible for malignant tumor progression and metastasis. Besides its involvement in apoptosis, only few studies on the effect of Bcl-2 on cancer metastasis, has been reported. As **IPTBC** acts as a feasible Bcl-2 inhibitor, to confirm that reduced levels of Bcl-2 can lessen the migratory potential of cancer cells [37], scratch wound migration assay was done in MCF-7 cells. Fig 8 displays the wound gap during wound generation and after 24 h in vehicle control, positive control vincristine and **IPTBC** treated MCF-7 cells. The figure evidently points towards the efficacy of **IPTBC** in intensely restricting cell migration. After 24 h treatment with **IPTBC**, the MCF- cells are less motile and could not close the wound gap.

Fig.8

4. Conclusion

Three new indole-coumarin-thiadiazole derivatives were synthesized by utilizing a pharmacophoric hybridization approach. The data from *in vitro* experiments showed that hybrid **IPTBC** exhibits differential cytotoxicity in MCF-7 cells and the cell kill was through apoptotic mode. The results of the current study imply that **IPTBC** can possibly act as chemotherapeutic agent specific to breast cancer both by the induction of apoptosis and by preventing metastasis. Further research is desirable to understand and strengthen the complete mechanism of **IPTBC**.

Acknowledgement:

The authors are thankful to Department of Science and Technology, Science and Engineering Research Board, India, for supporting the computational facilities through Grant SB/FT/LS-273/2012. One of the authors (P.R.K) is thankful to the Director, Manipal Institute of Technology, Manipal University for providing the necessary laboratory facilities and Dr. T.M.A - Pai Ph.D scholarship.

Reference

- [1] J.L. Koff, S. Ramachandiran, L. Bernal-Mizrachi, A time to kill: targeting apoptosis in cancer, *Int. J. Mol. Sci.* 16 (2015) 2942-2955.
- [2] A.B. Parrish, C.D. Freel, S. Kornbluth, Cellular mechanisms controlling caspase activation and function, *Cold Spring Harb. Perspect. Biol.* 5 (2013).

- [3] J. Vogel, X. Wang, A. Troxel, C.B. Simone, 2nd, R. Rengan, L.L. Lin, Prospective assessment of demographic characteristics associated with worse health-related quality of life measures following definitive chemoradiation in patients with locally advanced non-small cell lung cancer, *Int. J. Radiat. Oncol. Biol. Phys.* 96 (2016) S199-S200.
- [4] J.C. Evans, C. Trujillo, Z. Wang, H. Eoh, S. Ehrt, D. Schnappinger, H.I. Boshoff, K.Y. Rhee, C.E. Barry 3rd, V. Mizrahi, Validation of CoaBC as a bactericidal target in the coenzyme A pathway of *Mycobacterium tuberculosis*, *ACS Infect. Dis.* 2(12) (2016) 958-968.
- [5] G. Pistritto, D. Trisciuglio, C. Ceci, A. Garufi, G. D'Orazi, Apoptosis as anticancer mechanism: function and dysfunction of its modulators and targeted therapeutic strategies, *Aging* 8 (2016) 603-619.
- [6] P. Asadi, G. Khodarahmi, A. Jahanian-Najafabadi, L. Saghaie, F. Hassanzadeh, Biologically active heterocyclic hybrids based on quinazolinone, benzofuran and imidazolium moieties: synthesis, characterization, cytotoxic and antibacterial evaluation, *Chem. Biodivers.* (2016), DOI: 10.1002/cbdv.201600411.
- [7] S. Haider, M.S. Alam, H. Hamid, 1,3,4-Thiadiazoles: a potent multi targeted pharmacological scaffold, *Eur. J. Med. Chem.* 92 (2015) 156-177.
- [8] A. Senff-Ribeiro, A. Echevarria, E. Silva, C. Franco, S. Veiga, M. Oliveira, Cytotoxic effect of a new 1, 3, 4-thiadiazolium mesoionic compound (MI-D) on cell lines of human melanoma, *Br. J. Cancer* 91 (2004) 297-304.
- [9] B. Masereel, S. Rolin, F. Abbate, A. Scozzafava, C.T. Supuran, Carbonic anhydrase inhibitors: anticonvulsant sulfonamides incorporating valproyl and other lipophilic moieties, *J. Med. Chem.* 45 (2002) 312-320.
- [10] R. Pingaew, A. Saekee, P. Mandi, C. Nantasenamat, S. Prachayasittikul, S. Ruchirawat, V. Prachayasittikul, Synthesis, biological evaluation and molecular docking of novel chalcone-coumarin hybrids as anticancer and antimalarial agents, *Eur. J. Med. Chem.* 85 (2014) 65-76.
- [11] M. Roussaki, K. Zelianios, E. Kavetsou, S. Hamilakis, D. Hadjipavlou-Litina, C. Kontogiorgis, T. Liargkova, A. Detsi, Structural modifications of coumarin derivatives: Determination of antioxidant and lipoxygenase (LOX) inhibitory activity, *Bioorg. Med. Chem.* 22 (2014) 6586-6594.
- [12] T. Nasr, S. Bondock, M. Youns, Anticancer activity of new coumarin substituted hydrazide-hydrazone derivatives, *Eur. J. Med. Chem.* 76 (2014) 539-548.

- [13] S. Sandhu, Y. Bansal, O. Silakari, G. Bansal, Coumarin hybrids as novel therapeutic agents, *Bioorg. Med. Chem.* 22 (2014) 3806-3814.
- [14] A. Kamal, M. Rao, P. Das, P. Swapna, S. Polepalli, V.D. Nimbarte, K. Mullagiri, J. Kovvuri, N. Jain, Synthesis and biological evaluation of imidazo [2, 1-b][1, 3, 4] thiadiazole-linked oxindoles as potent tubulin polymerization inhibitors, *ChemMedChem* 9 (2014) 1463-1475.
- [15] P.R. Kamath, D. Sunil, A.A. Ajees, K. Pai, S. Das, Some new indole-coumarin hybrids; Synthesis, anticancer and Bcl-2 docking studies, *Bioorg. Chem.* 63 (2015) 101-109.
- [16] J. van Meerloo, G.J. Kaspers, J. Cloos, Cell sensitivity assays: the MTT assay, *Methods Mol. Biol.* 731 (2011) 237-245.
- [17] K. Liu, P.C. Liu, R. Liu, X. Wu, Dual AO/EB staining to detect apoptosis in osteosarcoma cells compared with flow cytometry, *Med. Sci. Monit. Basic. Res.* 21 (2015) 15-20.
- [18] M.M. Joseph, S.R. Aravind, S. Varghese, S. Mini, T.T. Sreelekha, PST-Gold nanoparticle as an effective anticancer agent with immunomodulatory properties., *Colloids. Surf. B. Biointerfaces.* 104 (2013) 32-39.
- [19] M.M. Joseph, S.K. George, K.R. Pillai, S. Mini, T.T. Sreelekha, Galactoxyloglucan-modified nanocarriers of doxorubicin for improved tumor-targeted drug delivery with minimal toxicity, *J. Biomed. Nanotechnol.* 10 (2014) 3253-3268.
- [20] B.N. Jyothi, M. Saswat, M. Safeera, G. Surajit, T.T. Sreelekha, K.K. Maiti, A dual-targeting octaguanidine-doxorubicin conjugate transporter for inducing caspase-mediated apoptosis on folate-expressing cancer cells, *ChemMedChem.* 11 (2016) 702-712.
- [21] M. Vaid, T. Singh, S.K. Katiyar, Grape seed proanthocyanidins inhibit melanoma cell invasiveness by reduction of PGE2 synthesis and reversal of epithelial-to-mesenchymal transition, *PLoS One* 6 (2011) e21539.
- [22] O. Trott, A.J. Olson, AutoDock Vina: improving the speed and accuracy of docking with a new scoring function, efficient optimization and multithreading, *J. Comput. Chem.* 31 (2010) 455-461.
- [23] G.M. Morris, R. Huey, W. Lindstrom, M.F. Sanner, R.K. Belew, D.S. Goodsell, A.J. Olson, AutoDock4 and AutoDockTools4: Automated docking with selective receptor flexibility, *J. Comput. Chem.* 30 (2009) 2785-2791.

- [24] A.G. Ali, M.F. Mohamed, A.O. Abdelhamid, M.S. Mohamed, A novel adamantane thiadiazole derivative induces mitochondria-mediated apoptosis in lung carcinoma cell line, *Bioorg. Med. Chem.* 25 (2017) 241-253.
- [25] X. Wu, Y. Fu, X. Sun, C. Liu, M. Chai, C. Chen, L. Dai, Y. Gao, H. Jiang, J. Zhang, The possible FAT1-mediated apoptotic pathways in porcine cumulus cells, *Cell. Biol. Int.* 41 (2017) 24-32.
- [26] L. Chen, S.N. Willis, A. Wei, B.J. Smith, J.I. Fletcher, M.G. Hinds, P.M. Colman, C.L. Day, J.M. Adams, D.C. Huang, Differential targeting of prosurvival Bcl-2 proteins by their BH3-only ligands allows complementary apoptotic function, *Mol. Cell.* 17 (2005) 393-403.
- [27] S.K. Tahir, X. Yang, M.G. Anderson, S.E. Morgan-Lappe, A.V. Sarthy, J. Chen, R.B. Warner, S.-C. Ng, S.W. Fesik, S.W. Elmore, Influence of Bcl-2 family members on the cellular response of small-cell lung cancer cell lines to ABT-737, *Cancer. Res.* 67 (2007) 1176-1183.
- [28] C. Tse, A.R. Shoemaker, J. Adickes, M.G. Anderson, J. Chen, S. Jin, E.F. Johnson, K.C. Marsh, M.J. Mitten, P. Nimmer, L. Roberts, S.K. Tahir, Y. Xiao, X. Yang, H. Zhang, S. Fesik, S.H. Rosenberg, S.W. Elmore, ABT-263: a potent and orally bioavailable Bcl-2 family inhibitor, *Cancer Res.* 68 (2008) 3421-3428.
- [29] A.J. Souers, J.D. Levenson, E.R. Boghaert, S.L. Ackler, N.D. Catron, J. Chen, B.D. Dayton, H. Ding, S.H. Enschede, W.J. Fairbrother, D.C. Huang, S.G. Hymowitz, S. Jin, S.L. Khaw, P.J. Kovar, L.T. Lam, J. Lee, H.L. Maecker, K.C. Marsh, K.D. Mason, M.J. Mitten, P.M. Nimmer, A. Oleksijew, C.H. Park, C.M. Park, D.C. Phillips, A.W. Roberts, D. Sampath, J.F. Seymour, M.L. Smith, G.M. Sullivan, S.K. Tahir, C. Tse, M.D. Wendt, Y. Xiao, J.C. Xue, H. Zhang, R.A. Humerickhouse, S.H. Rosenberg, S.W. Elmore, ABT-199, a potent and selective BCL-2 inhibitor, achieves antitumor activity while sparing platelets, *Nat Med*, 19 (2013) 202-208.
- [30] P. Antonietti, F. Gessler, H. Dussmann, C. Reimertz, M. Mittelbronn, J.H. Prehn, D. Kogel, AT-101 simultaneously triggers apoptosis and a cytoprotective type of autophagy irrespective of expression levels and the subcellular localization of Bcl-xL and Bcl-2 in MCF7 cells, *Biochim. Biophys. Acta.* 1863 (2016) 499-509.
- [31] K.M. Boatright, G.S. Salvesen, Mechanisms of caspase activation, *Curr. Opin. Cell. Biol.* 15 (2003) 725-731.
- [32] A. Ashkenazi, V.M. Dixit, Death receptors: signaling and modulation, *Science.* 281 (1998) 1305-1308.

- [33] C.V. Kavitha, M. Nambiar, C.S. Ananda Kumar, B. Choudhary, K. Muniyappa, K.S. Rangappa, S.C. Raghavan, Novel derivatives of spirohydantoin induce growth inhibition followed by apoptosis in leukemia cells, *Biochem. Pharmacol.* 77 (2009) 348-363.
- [34] P. Dumont, L. Ingrassia, S. Rouzeau, F. Ribaucour, S. Thomas, I. Roland, F. Darro, F. Lefranc, R. Kiss, The Amaryllidaceae isocarbostryl narciclasine induces apoptosis by activation of the death receptor and/or mitochondrial pathways in cancer cells but not in normal fibroblasts, *Neoplasia* 9 (2007) 766-776.
- [35] S.P. Cullen, S.J. Martin, Caspase activation pathways: some recent progress, *Cell. Death. Differ.* 16 (2009) 935-938.
- [36] A.K. Mukherjee, A.J. Saviola, P.D. Burns, S.P. Mackessy, Apoptosis induction in human breast cancer (MCF-7) cells by a novel venom L-amino acid oxidase (Rusvinoxidase) is independent of its enzymatic activity and is accompanied by caspase-7 activation and reactive oxygen species production, *Apoptosis* 20 (2015) 1358-1372.
- [37] B.C. Koehler, A.L. Scherr, S. Lorenz, T. Urbanik, N. Kautz, C. Elssner, S. Welte, J.L. Bermejo, D. Jager, H. Schulze-Bergkamen, Beyond cell death - antiapoptotic Bcl-2 proteins regulate migration and invasion of colorectal cancer cells in vitro, *PLoS One* 8 (2013) e76446.

Legends

Scheme-1: Synthetic pathway for the preparation of thiadiazole derivatives

Fig. 1: Representative images of induction of apoptosis in MCF-7 cells on **IPtBC** treatment for 24 h. AO stains both live and dead cells, whereas EtBr dyes only apoptotic cells. A) Live cells in vehicle control appeared uniformly fluorescent green. B) **IPtBC** treated cells which are in early apoptosis phase are stained yellowish green with bright green dots in the nuclei, whereas the late apoptotic cells with condensed and fragmented nuclei incorporate EtBr and are stained red/orange. Hoechst staining of C) Vehicle control cells with round and intact nuclei and D) Apoptotic cells with signs of fragmented and condensed nuclei. Scale bar corresponds to 50 μm .

Fig. 2: Representative images of MCF-7 cells: Vehicle control and treated with **IPtBC** for 24 h in TUNEL assay. Cells that exhibited green fluorescence indicate apoptotic DNA fragmentation. Scale bar corresponds to 50 μm .

Fig. 3: Photomicrograph showing A) Vehicle control cells that are left unstained and B) Apoptotic cells that are stained intensely purple-red on exposure to **IPtBC**. Scale bar corresponds to 50 μm . C) Graph depicting the increase in absorbance in the case of MCF-7 cells exposed to **IPtBC** compared to vehicle control cells underlying the induction of apoptosis.

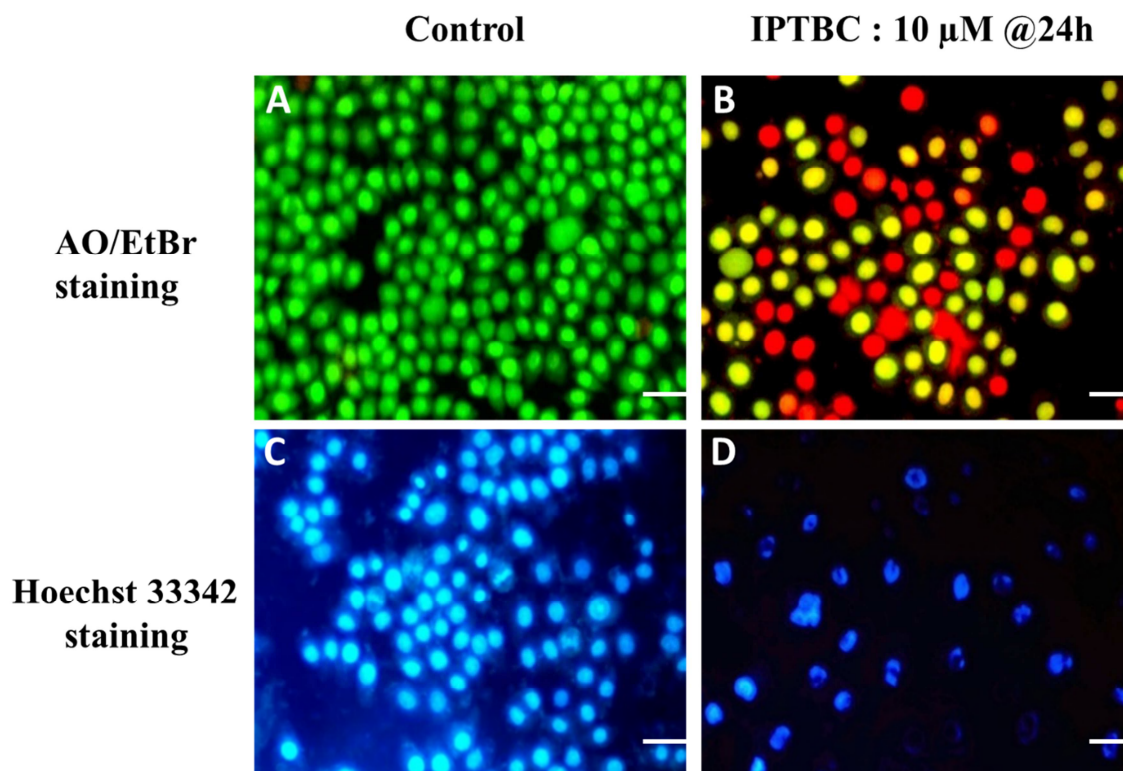
Fig. 4: Caspase activity profile related to apoptosis in **IPtBC** (10 μM) treated cells after 24 h. Data represented as mean \pm SD of three independent trials.

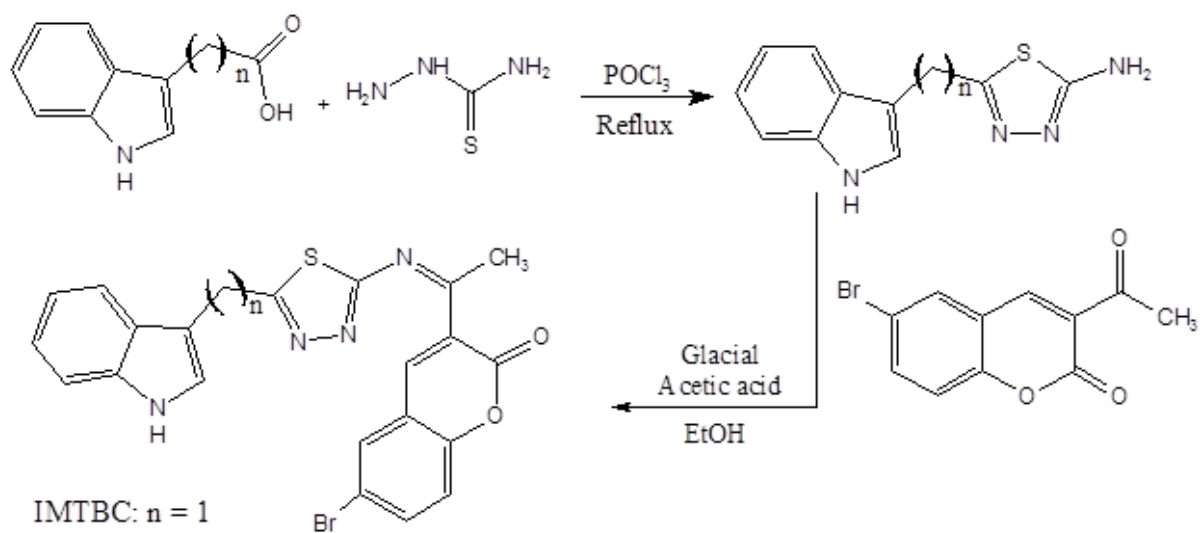
Fig. 5: Molecular Interactions of **IPTBC** with Bcl-2 drawn using (A) pymol and (B) PoseView. Bcl-2 amino acids and **IPTBC** are coloured cyan and green respectively and are shown as sticks. H-bonds are represented in solid in A and dotted lines in B. Hydrophobic interactions and π -stacking are presented in dotted lines in A.

Fig. 6: Binding mode of **IPTBC** and BH-3 protein in the BH-3 binding domain of Bcl-2. Bcl-2 is shown in surface and colored cyan. The **IPTBC** is depicted in sticks and BH-3 molecule is shown as a cartoon with 50% transparency, and colored green. The thiadiazole and indole moieties of **IPTBC** occupy the BH3 binding pocket. The presence of **IPTBC** in the binding pocket of Bcl-2 thus evidently restricts the binding of BH3.

Fig.7: Proposed mechanism for induction of apoptosis by **IPTBC**

Fig. 8: Wound gap immediately after wound generation and at 24 h and 48 h after treatment. Reduced migration of cells when treated with **IPTBC** compared to vehicle control is observed.



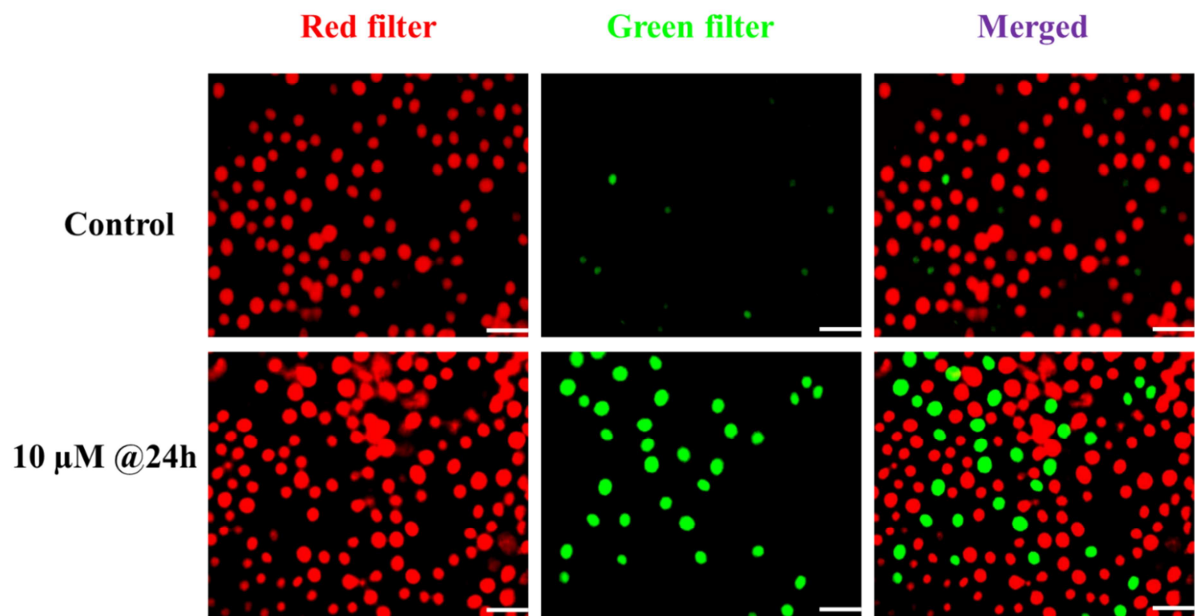


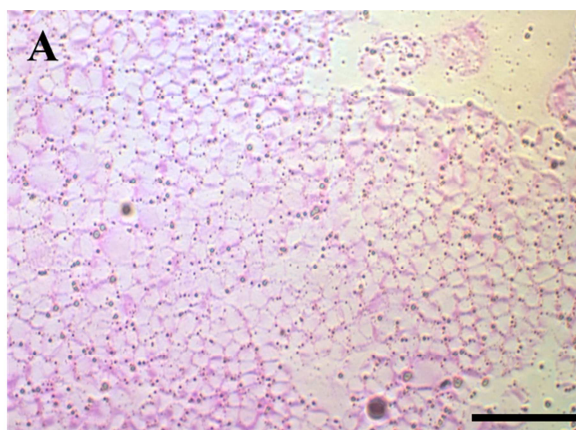
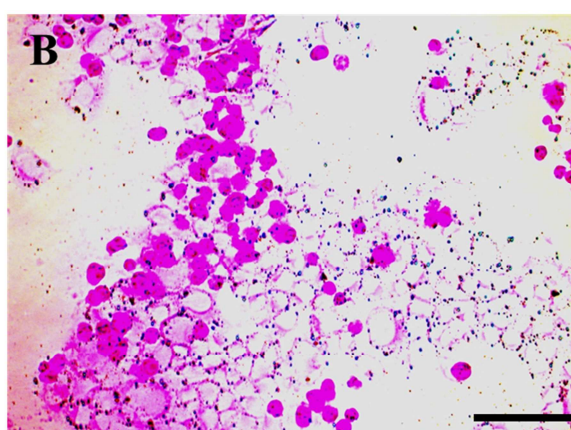
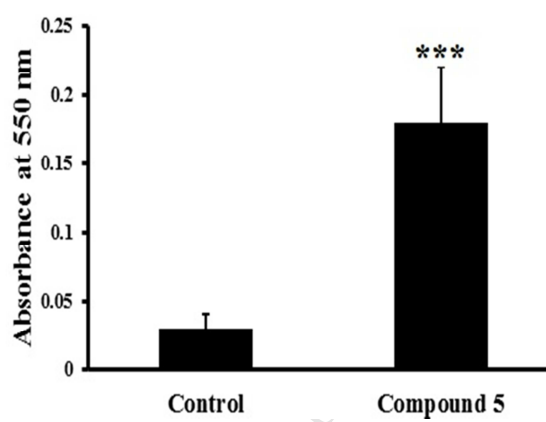
IMTBC: $n = 1$

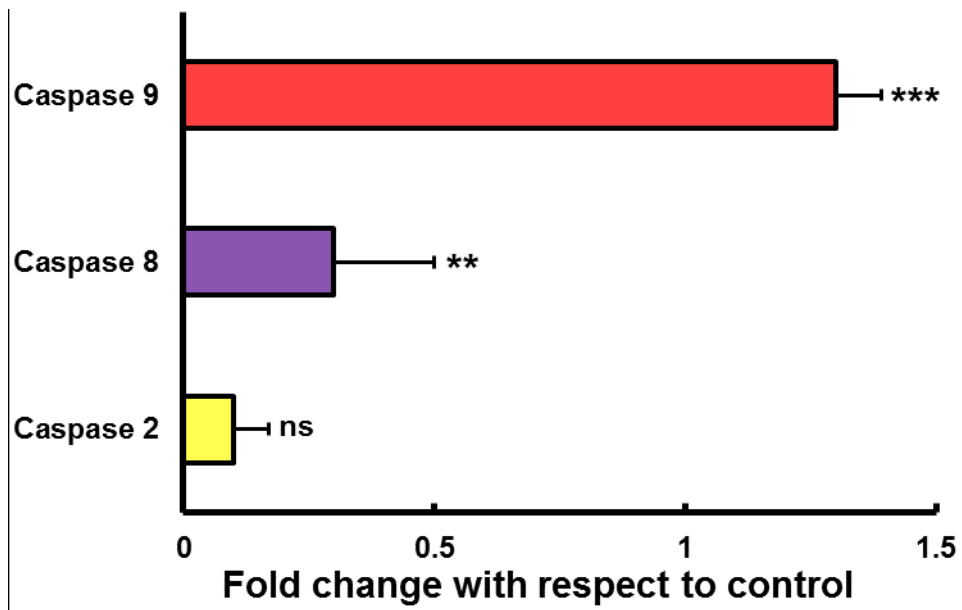
IETBC: $n = 2$ and

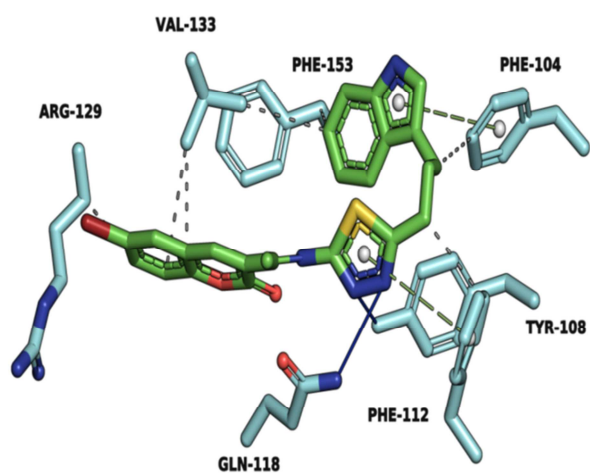
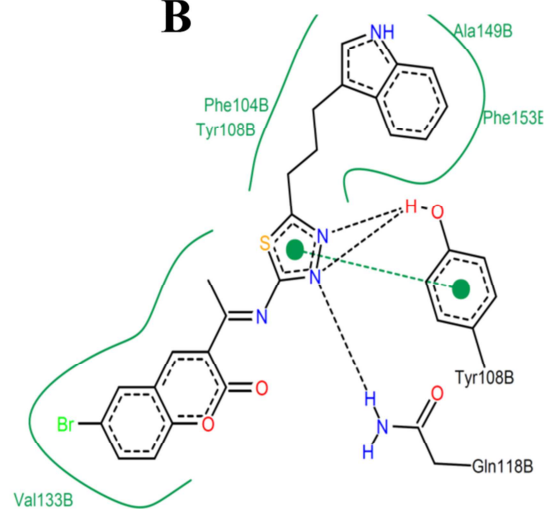
IPTBC: $n = 3$

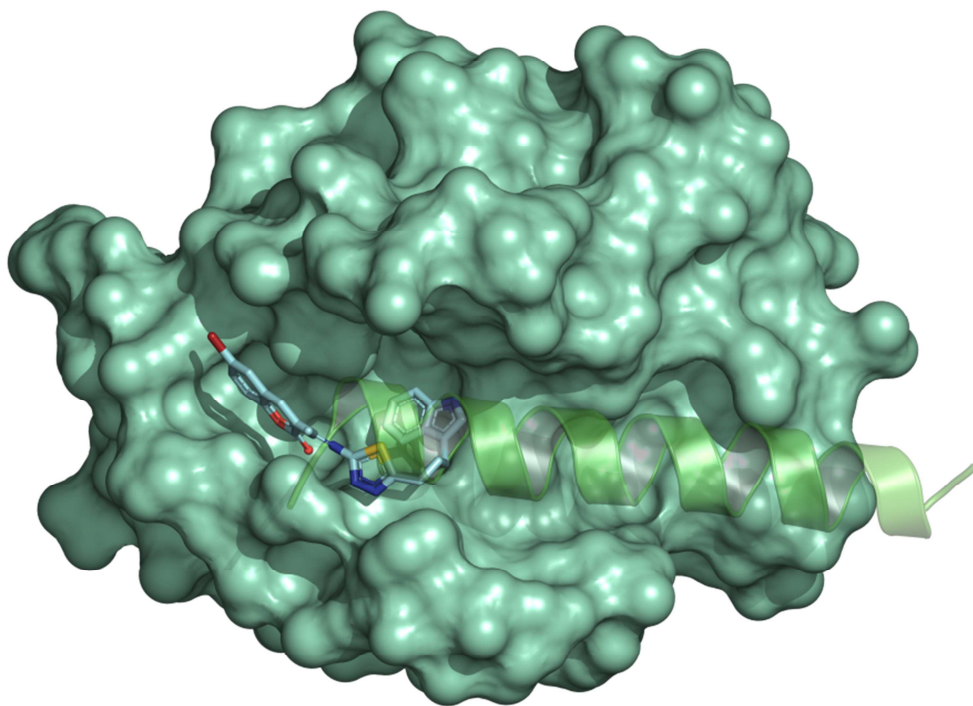
ACCEPTED MANUSCRIPT



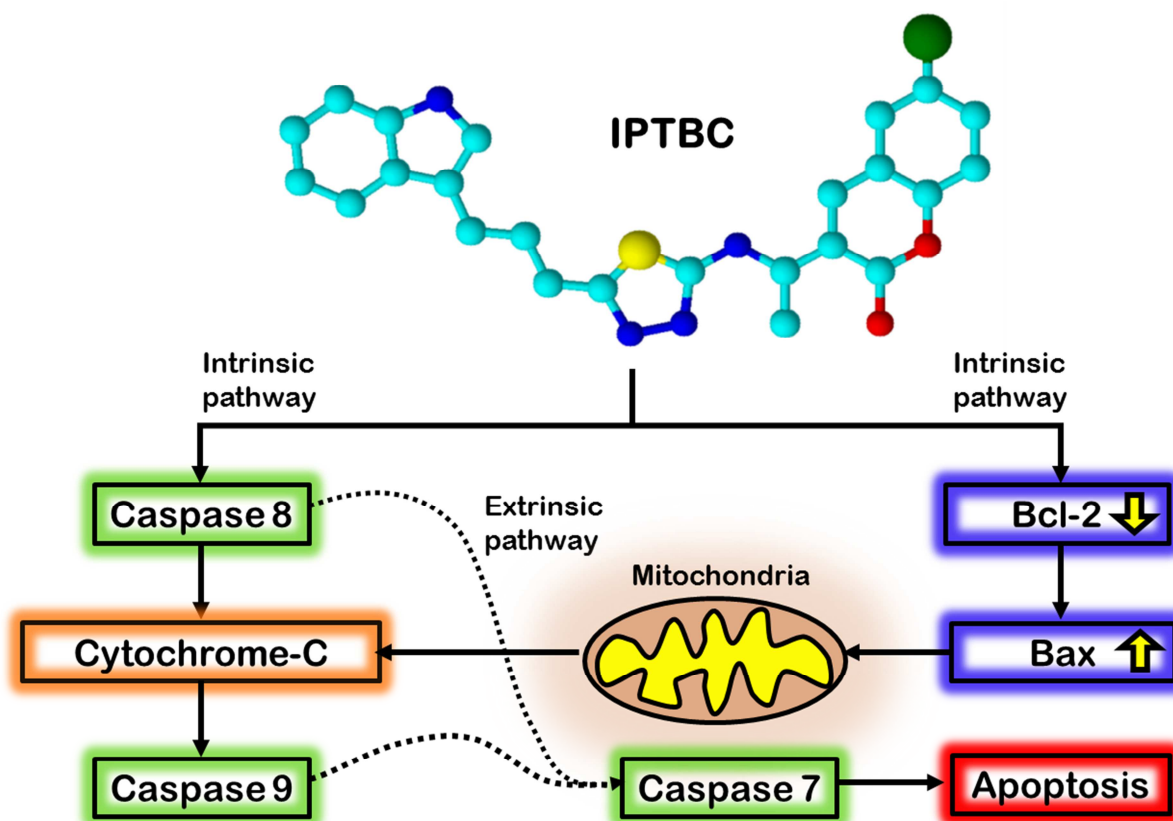
Control**10 μ M @24h****C**
**Colorimetric
quantitation**

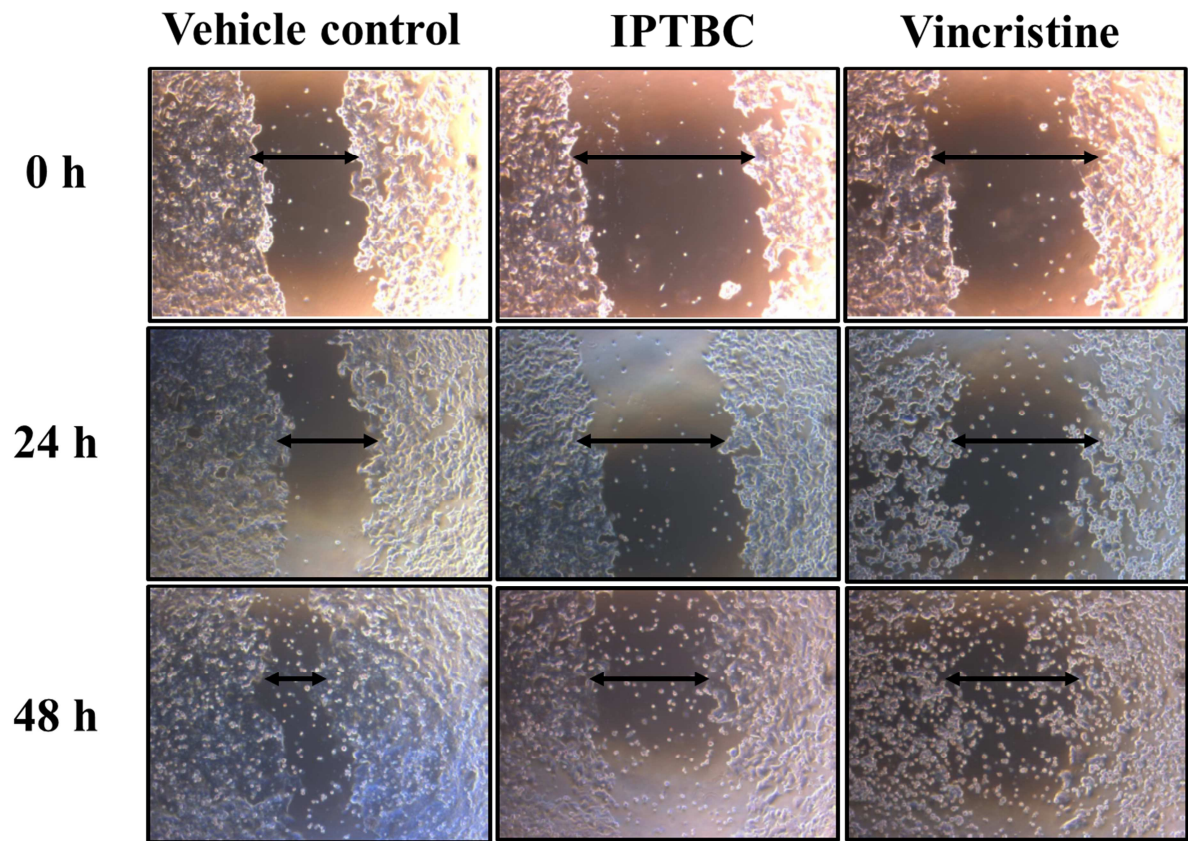


A**B**



ACCEPTED MANUSCRIPT





ACCEPTED MANUSCRIPT

Highlights

- Three new thiadiazole hybrids incorporating bioactive coumarin and indole scaffolds were synthesized.
- A new apoptotic and antimetastatic agent, **IPBC** was identified with significant differential toxicity towards MCF-7 cells.
- Docking studies recognised **IPBC** to bind well with the BH3 binding domain of Bcl-2.